Automatic segmentation of fish midlines for optimizing robot design

Fetherstonhaugh, Samuel E.A.W.; Shen, Qiang; Akanyeti, Otar

Published in:
Bioinspiration and Biomimetics

DOI:
10.1088/1748-3190/abf031

Publication date:
2021

Citation for published version (APA):
Fetherstonhaugh, S. E. A. W., Shen, Q., & Akanyeti, O. (2021). Automatic segmentation of fish midlines for optimizing robot design. *Bioinspiration and Biomimetics*, *16*(4), [046005]. https://doi.org/10.1088/1748-3190/abf031

Automatic segmentation of fish midlines for optimizing robot design

Bioinspiration & Biomimetics

OPEN ACCESS

PAPER

Automatic segmentation of fish midlines for optimizing robot design

Samuel E A W Fetherstonhaugh, Qiang Shen and Otar Akanyeti*

Department of Computer Science, Aberystwyth University, Ceredigion, SY23 3FL, United Kingdom
* Author to whom any correspondence should be addressed.

E-mail: ota1@aber.ac.uk

RECEIVED
13 January 2021

ACCEPTED FOR PUBLICATION
18 March 2021

PUBLISHED
20 May 2021

Keywords: fish robots, undulatory kinematics, multi-segment model, carangiform swimmers, steady swimming

Supplementary material for this article is available online

Abstract

While fish use continuous and flexible bodies to propel themselves, fish robots are often made from interconnected segments. How many segments do robots need to represent fish movements accurately? We propose a new method to automatically determine parsimonious robot models from actual fish data. We first identify key bending points (i.e., joint positions) along the body and then study the concerted movement of the segments so that the difference between actual fish and modelled bending kinematics is minimized. To demonstrate the utility of our method, we analyse the steady swimming kinematics of 10 morphologically distinct fish species. Broadly classified as sub-carangiform (e.g., rainbow trout) and carangiform (e.g., crevalle jack) swimmers, these species exhibit variations in the way they undulate when traditional parameters (including head and tail beat amplitudes, body wavelength and maximum curvature along the body) are considered. We show that five segments are sufficient to describe the kinematics with at least 99% accuracy. For optimal performance, segments should progressively get shorter towards the tail. We also show that locations where bending moments are applied vary among species, possibly because of differences in morphology. More specifically, we find that wider fish have shorter head segments. We discover that once bending points are factored in, the kinematics differences observed in these species collapse into a single undulatory pattern. The amplitude and timing of how body segments move entirely depend on their respective joint positions along the body. Head and body segments are also coupled in a timely manner, which depends on the position of the most anterior joint. Our findings provide a mechanistic understanding of how morphology relates to kinematics and highlight the importance of head control, which is often overlooked in current robot designs.

1. Introduction

In contrast to man-made propellers, most fish produce thrust by undulating their axial bodies (Bainbridge 1963). In recent years, there has been a significant push to build robots that can swim like fish. However, this is a challenging task. While fish are flexible and have high degrees of freedom at the same time (Wardle *et al* 1995, Jayne and Lauder 1995, Altringham and Ellerby 1999), fish robots are often made from multiple segments with rigid (to accommodate batteries, electronics, sensors, motors and cables) and compliant parts (to replicate the bending movements of the posterior body and caudal fin). When speed, efficiency and manoeuverability are considered, fish robots are not as good as their biological counterparts and have low technology readiness levels as compared to traditional propeller-driven autonomous or remotely operated underwater vehicles (Eriksen *et al* 2001, Ribas *et al* 2011).

Given technological limitations, body design is a research area that can benefit from a formalized approach while drawing inspiration from biology. This is of particular significance to address questions like: how do we partition the body and where do we place actuation points so that the movements of a robot resemble those of the fish that it is designed after? What is the most parsimonious robot design (design with the smallest number of segments) that can describe the movements of the fish accurately?

Does one design fit all or how should it vary while modelling different behaviours or fish species?

Actual fish movements are seldomly reported in the literature, and traditional kinematics measurements used by biologists to describe these movements (e.g., head and tail amplitudes, tail beat frequency, body wavelength and maximum curvature) do not lend themselves well to provide pragmatic mechanical engineering guidelines. To mitigate this problem up to a certain extent, many research groups use artificial body midlines generated by a travelling wave equation as a proxy to study fish movements (Liu and Hu 2006, Yu *et al* 2007, Zhong *et al* 2017):

$$h(x) = a(x) * \sin(kx - wt), \tag{1}$$

where t is the time stamp, x is the position of the midline point along the body, $w = 2\pi f$ (f is the tail beat frequency), $k = \frac{2\pi}{\lambda}$ (λ is the body wavelength) and $a(x) = C_1 x + C_2 x^2$. The equation parameters (C_1, C_2 and λ) control how the body bends and can be customized for different swimming modes. The majority of robots are designed after sub-carangiform (e.g., rainbow trout, *Oncorhynchus mykiss*, in Krusmaa *et al* (2014)) and carangiform (e.g., common carp, *Cyprinus carpio*, in Ozmen Koca *et al* (2018)) swimmers; hereinafter we will refer to these two groups as (sub-)carangiform swimmers. In these designs, it is widely assumed that undulatory movements are largely confined to the posterior body, with body amplitudes increasing exponentially towards the tail and body wavelength being around one. Once the artificial midlines are generated according to these criteria, they are used to identify the key bending points to orient robot design.

The travelling wave equation is a good first step in modelling fish swimming, however it has certain limitations. First, there is very little empirical data on how well the midlines generated by the travelling wave equation approximate the actual midlines of fish during steady swimming (Videler and Hess 1984, Tytell and Lauder 2004). Second, it does not specify how the head moves nor where the body wave starts, as both parameters play key roles in swimming performance and vary among species (Lindsey 1978). Third, further studies are needed to evaluate whether the travelling wave equation can be modified to approximate other behaviours observed during turning, C-start, linear acceleration and swimming in unsteady flows, see (Akanyeti and Liao 2013) for modelling Kármán gaiting.

In this work, we propose a new method which enables roboticists to draw conclusions from real fish data. Assuming that fish movements can be represented with a series of linear segments, the proposed method first identifies the minimum number of segments that can describe fish movements accurately, and then identifies a control architecture which describes the concerted movement of these segments so that the difference between actual and modelled kinematics is minimized. We demonstrate the utility of our method by studying the steady swimming kinematics of 10 representative species from (sub-) carangiform swimmers with distinct body shapes and flexural stiffness.

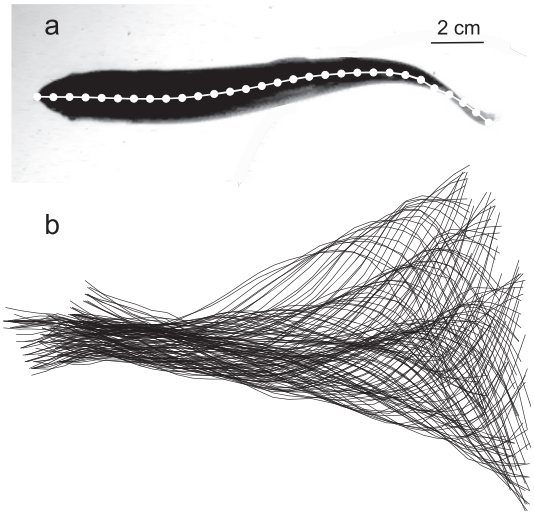

Figure 1. (a) A snapshot of a rainbow trout ($L = 23$ cm) during steady swimming at around 2 $L\,s^{-1}$ in a flow tunnel (ventral view). Body midline (white line) and digitized points (white circles) are superimposed on top. Flow direction is from left to right. (b) Body midlines from same fish over three tail beats.

2. Methods

2.1. Problem definition

The input data consists of body midlines which are represented in the form of three-dimensional matrices, $M(x, y, t)$, describing how points along the body (x, y) move in time (t). The data comes from actual fish experiments captured by a high-speed camera with the image plane parallel to the direction of motion (figure 1). Here, we assume that the fish midline points translate and rotate in two dimensions within the imaging plane without rolling, pitching and/or twisting movements. To represent midlines using a multi-segment model we propose two methods (namely, segment growing method and genetic algorithm) to meet the needs of roboticists in two complementary ways. In particular, the segment growing method determines the minimum number of segments required to achieve a certain degree of modelling accuracy (defined by the user *a priori*), whereas the genetic algorithm is devised to work with a fixed number of segments (defined by the user *a priori*), calculating the optimal lengths of these segments to maximize accuracy.

2.2. Segment growing method

Starting from the most anterior midline point, we create the first segment (S_1) with an initial length S_{init}. We grow S_1 with finite increments (ΔS) until

Table 1. Segment growing algorithm; where S_{init} and ΔS refer to initial segment length and a finite increment in segment length, respectively. Algorithm inputs (fish midlines and error threshold), output (joint positions) and variables (S_{init} and ΔS) are all normalized to the body length.

```
Algorithm segmentGrowing()
Inputs: fish midlines (M), error threshold (eTh)
Outputs: joint locations (J)
Variables: S_init, ΔS
J = [], S_b = 0, S_e = S_init
while S_e < 1
 E = calculateSegmentError (S_e, S_b, M)
 if E < eTh
  S_e += ΔS
 else
  S_b = S_e − ΔS
  S_e = S_b + S_init
  add S_b to J
 end
end
return J
```

the mean difference between S_1 and the actual midline exceeds the error threshold (supplementary figure 1 (https://stacks.iop.org/BB/16/046005/mmedia)). At this point, we stop growing S_1 and create a joint (J_1). We then start growing the second segment (S_2) from J_1 until the mean difference between S_2 and the actual midline exceeds the error threshold, and this iterative process continues until we reach the most posterior point along the body. At the end, the segment growing method produces a number of segments with variable lengths, each of which describes a finite portion of the actual midline.

2.2.1. Calculation of individual segment error

For all time frames, $t = \{1, 2, 3, \ldots, T\}$, we calculate the difference between the segment S_i and the corresponding portion of the fish midline M_i by measuring the perpendicular distance for each midline point (x_j, y_j) that belongs to M_i,

$$D_{ij} = \frac{|\,(y_{ie} - y_{ib}) \times x_j - (x_{ie} - x_{ib}) \times y_j + x_{ib} \times y_{ie} - x_{ie} \times y_{ib}|}{\sqrt{(x_{ie} - x_{ib})^2 + (y_{ie} - y_{ib})^2}} \tag{2}$$

where $S_{ib} = (x_{ib}, y_{ib})$ and $S_{ie} = (x_{ie}, y_{ie})$ denote the beginning and end points of the segment S_i, respectively and $x_{ib} < x_j < x_{ie}$. We then take the maximum distance (among the midline points) and average it over time to arrive at the final segment error (or mean difference),

$$E_i = \frac{1}{t}\sum_{t=1}^{T} \max_{j \in M_i} D_{ij}. \tag{3}$$

For each time frame, S_{ib} and S_{ie} are derived from the joint positions (e.g., 0 and J_1 for S_1, J_1 and J_2 for S_2, and so on) by transforming the data from one to two dimensions so that they are mapped on to the curvilinear fish midline. The beginning of the first segment is initialized to the most anterior midline point. Similarly, the end of the last segment is fixed at the most posterior midline point.

2.2.2. Overall performance of multi-segment model

From all segments constituting the model $\hat{M}$, we choose the one with a maximum mean difference to summarize the overall performance (supplementary figure 2)

$$\hat{E} = \max_{i \in \hat{M}} E_i. \tag{4}$$

The lower the error, the better the performance. Putting it another way, we equate the overall accuracy of the model to the accuracy of the worst performing segment (i.e., the weakest link).

Segment growing method guarantees parsimonious segment formations through locally optimal decisions, i.e., by finding the longest segment with an error below the desired threshold, for each portion of the fish midline. In this way, it is also guaranteed that the overall model error is kept below the threshold. A greedy algorithm for segment growing method is given in table 1.

2.3. Genetic algorithm

The genetic algorithm starts with a fixed number of segments and uses heuristic search to determine the optimal segment lengths so that the overall model performance is maximized, similar to the approach of Bal *et al* (2016). Beginning with an initial population of random solutions, the genetic algorithm draws principles from the theory of evolution and natural selection where fittest solutions are selected for producing candidate solutions of the next generation. Such an iterative process continues for a fixed number of generations or until an optimality criterion is reached. The genetic algorithm is a popular method in computer science and there are many ways of implementing it (Whitley 1994). Here, we briefly describe the implementation tailored to our problem.

2.3.1. Initialization

In our representation, a solution is a vector of joints connecting the actual segments $(J_1, J_2, \ldots, J_{S-2}, J_{S-1}$

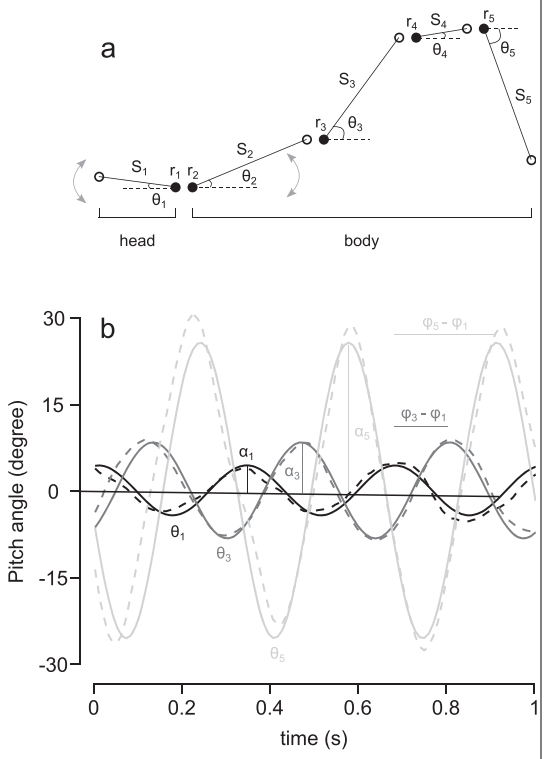

Figure 2. Controlling segments. (a) Illustration of a five-segment model (not drawn to scale) including the head (S_1) and body segments ($S_2 - S_5$). Each segment, i, (black line) rotates around an anchor point (filled black circle) where pitch angles are denoted by (θ_i). Segment ends are indicated by empty circles. (b) Pitch angles over three tail beats for S_1 (black), S_3 (dark grey) and S_5 (light grey) are shown as an example where actual measurements and their sine wave approximations are plotted using dashed and solid lines, respectively. Sine wave parameters, pitch amplitude (α_i) and relative timing with respect to the head segment $\varphi_i - \varphi_1$ are also shown.

where S is the number of segments). Each joint has a value between 0 and 1L (indicating the position along the body with L standing for the body length). Each generation consists of a fixed number of candidate solutions (N_{sol}) that are evaluated together, and the goodness (or fitness) of a solution is calculated using the weakest link approach as previously described in section 2.2.2. In the first generation, we initialize the joint positions (of each solution) quasi-randomly. We apply a constraint to maintain an ascending order in the joint positions (i.e., $J_1 < J_2 < \cdots < J_{S-2} < J_{S-1}$). In the second and following generations, we create candidate solutions (alternatively termed offsprings) from the solutions of the previous generation (parents) using four genetic operators: selection, cloning, crossover and mutation.

2.3.2. Parent selection

During the process of parent selection, we first rank the possible solutions according to their fitness scores and normalize the rankings (r) between 0 (lowest fitness score) and 1 (highest fitness score). Each solution has a probability (P) of being selected as a parent based on its fitness,

$$P = r^z, \tag{5}$$

where z determines the bias towards solutions with high fitness scores. In this approach, solutions are represented as portions in a pie chart and the size of the portion is proportional to the P. We then select parents using the classical roulette wheel method by generating a random number between 0 and 2π and select the solution that the number falls into.

2.3.3. Offspring creation

We select two parents for producing two offsprings, either by (1) cloning, where the resulting offsprings are identical copies of their parents (one offspring per parent), or (2) crossover, where the offsprings carry information from both parents. During crossover, we split parents into two parts (anterior and posterior joint positions) and the offsprings inherit one part from each parent. Offsprings are also allowed to have minute changes in the joint positions through mutations to maintain diversity and explore new solutions locally. The rate and degree of mutations are controlled by two independent parameters. We next filter out those offsprings with invalid joint positions (i.e., removing those joint positions that are either outside of the body limits or not in an ascending order). This iterative process continues until we generate a sufficient number of offsprings to fill the quota, N_{sol}.

2.4. Actuating segments

Once a multi-segment model is created (be it through the segment growing method or the genetic algorithm), the next step is to determine the control parameters that actuate these segments. In this study, we focus on the situation of steady swimming. We assume that each segment has one degree of freedom which rotates around a joint (pitching hereinafter) and the motion is periodic, which is a common architecture used in multi-segment fish robots, e.g., (Liu and Hu 2010). To describe the pitch angle, θ, of each segment, i, over time we use a sine equation

$$\theta_i = \alpha_i * \sin(\omega t + \varphi_i), \tag{6}$$

where two variables α and φ controlling the pitch amplitude and timing, respectively, t is the time stamp and $\omega = 2\pi f$ with f being the tail beat frequency. The theoretical basis for this representation comes from previous fish studies where lateral movements of each point along the midline is described using a Fourier series. In this representation, the most significant contribution coming from the first term oscillating at the tail beat frequency (Videler and Hess 1984, Root *et al* 2007, Akanyeti and Liao 2013). We first estimate f by analyzing the movements of the caudal fin over multiple tail beats. We then estimate α and φ (for each segment) using the method of least squares so that

the difference between measured and predicted θ is minimized.

At the end, we represent the kinematics of the S-segment model with $2S+1$ motion parameters $[f, \alpha_1, \varphi_1, \alpha_2, \varphi_2, \ldots, \alpha_{S-1}, \varphi_{S-1}, \alpha_S, \varphi_S]$ and S actuation points (distributed along the body) $[r_1, r_2, \ldots, r_{S-1}, r_S]$ which specify the points of rotation for each segment. We divide segments into two groups: head segment (the first segment, S_1) and body segments (starting from S_2) (figure 2). In this configuration, the head and the most anterior body segments rotate around the same point ($r_1 = r_2$) but they face opposite directions. To standardize pitch timing across datasets, we use the timing of the head movement as a reference to adjust the timing of body movements $[f, \alpha_1, 0, \alpha_2, \varphi_2 - \varphi_1, \ldots, \alpha_{N-1}, \varphi_{N-1} - \varphi_1, \alpha_N, \varphi_N - \varphi_1]$.

2.5. Datasets

We demonstrate the utility of our approach by analyzing two datasets from our previous work (Akanyeti *et al* 2017): (1) **trout dataset** which includes five rainbow trout swimming steadily at around 2 L s^{-1} ($L = 21.8 \pm 2.9$ cm), and (2) **multi-species dataset** which includes ten species swimming steadily (one fish and one speed per species). These species are Florida gar (*Lepisosteus platyrhincus*, $L = 36.9$ cm, 1 L s^{-1}), northern barracuda (*Sphyraena borealis*, $L = 33$ cm, 2.6 L s^{-1}), clown knifefish (*Chitala ornata*, $L = 19.4$ cm, 1.4 L s^{-1}), sheepshead (*Archosargus probatocephalus*, $L = 32$ cm, 1.8 L s^{-1}), crevalle jack (*Caranx hippos*, $L = 45.5$ cm, 3.1 L s^{-1}), mangrove snapper (*Lutjanus griseus*, $L = 23$ cm, 3.2 L s^{-1}), Indo-Pacific tarpon (*Megalops cyprinoides*, $L = 23$ cm, 2.7 L s^{-1}), tomtate (*Haemulon aurolineatum*, $L = 20$ cm, 1 L s^{-1}), pinfish (*Lagodon rhomboides*, $L = 28$ cm, 2.9 L s^{-1}) and rainbow trout ($L = 23$ cm, 3.4 L s^{-1}).

All fish data were collected using a high-speed camera (250 frames per second and a minimum of three tail beats per trial), where each frame was digitized to obtain 30 equally spaced x and y coordinates to represent the body midline.

2.6. Data analysis

Custom-written Octave and Matlab scripts are used to analyse the data. Midline data were normalized with respect to the body length L and all distance measures are reported in L. All results are shown as mean $\pm$ standard deviation of the mean, unless stated otherwise.

2.6.1. Parameter selection for segment growing method and genetic algorithm

Because each midline consists of 30 points, we fix S_{init} and ΔS at 0.033 L (for the segment growing method). Our initial investigation with preliminary data suggests that running the genetic algorithm for 10 generations and evaluating 200 solutions per generation (i.e., $N_{\text{sol}} = 200$) is sufficient to produce a meaningful solution in a reasonable amount of time (an example is shown in supplementary figure 3). The probability of crossover over cloning is set to 0.3. During crossover, parents with an even number of joints are divided into two equal halves whereas parents with an odd number of joints are divided into two parts where the anterior part has one extra joint. We equate z to 8. The rate and degree of mutation are fixed at 5% and 0.01L, respectively. During mutation, there is a 50–50 chance that the joint position would move in the anterior (or posterior) direction.

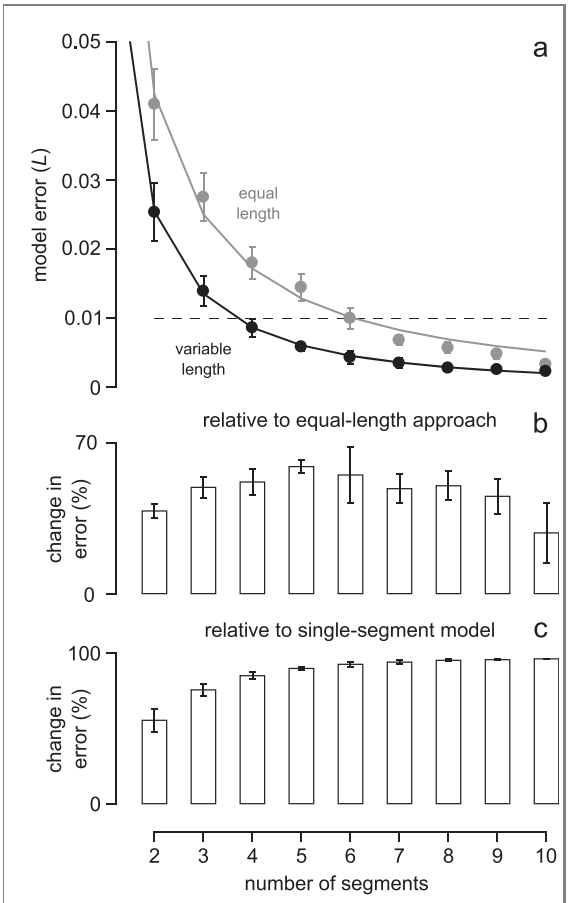

Figure 3. Performance of multi-segment models in describing fish steady swimming midlines (trout dataset). (a) Mean model error up to 10 segments; variable-length (black line $y = 0.1x^{-1.5}$, $R^2 = 0.95$) versus equal-length approach (gray, $y = 0.1x^{-1.3}$, $R^2 = 0.95$). 0.01L error line is shown as reference (dashed line). (b) Relative difference in mean error between variable-length and equal-length segment models. (c) Relative difference in mean error between variable-length segment models and single-segment models. All error bars indicate standard deviations from the mean.

2.6.2. Agreement between segment growing method and genetic algorithm

We first check whether the segment growing method and the genetic algorithm produce similar multi-segment models. We fit a linear regression comparing joint positions generated by these two methods and we calculate similarity using the slope of the regression and the coefficient of determination (namely, the R^2 value). We hypothesize that the slope and R^2 values will be close to one (which corresponds to perfect

match) indicating strong agreement between the two methods. We also visualize the Bland–Altman plot to evaluate the limit of agreement between two methods.

2.6.3. Change of model performance vs increasing number of segments

To estimate the relationship between the model performance (y) and the number of segments (x), we use a power equation

$$y = ax^b, \tag{7}$$

where the coefficients a and b are estimated using the least squares method. Assuming that the model error will decrease with respect to an increasing number of segments ($b < 0$), the magnitude of b indicates the decay constant. The goodness of the fit is evaluated by the R^2 value. We use both methods to systematically generate models with a different number of segments (up to 10 segments). In the segment growing method, we generate multiple models by systematically increasing the error threshold from $0.001L$ to $0.1L$ with $0.001L$ increments and select the model with the best overall performance (for each segment number). In the genetic algorithm, we simply enter the desired number of segments and the algorithm looks for the best combination of segment lengths to minimize the error.

2.6.4. Comparison with equal-length segment and single-segment models

Both the segment growing method and the genetic algorithm produce models that may have variable-length segments (variable-length segment models hereinafter). For instance, the model shown in the supplementary figure 1 has its first segment longer than the second segment, the second segment longer than the third segment, and so on. How important is it to have variable-length segments? To address this question, we compare the performance of the variable-length segment models to the models with equal-length segments. Equal-length segment models are often used in robot designs for simplicity and very few studies have formally investigated the efficacy of variable length approach (Yu *et al* 2007, Su *et al* 2014). We perform the comparison in two different ways. First, we repeat the analysis described in section 2.6.3 for the equal-length segment models. While increasing the number of segments, we predict that the error will decrease faster (i.e., with a larger magnitude of b) in the variable-length segment models than in equal-length segment models. Second, we calculate the relative change in error (Δe) using:

$$\Delta e = 100 * \left(1 - \frac{e_1}{e_2}\right), \tag{8}$$

where e_1 and e_2 are the errors of the variable-length and equal-length segment models, respectively, and Δe varies within the range of 0% (no change, $e_1 = e_2$) to 100% ($e_1 = 0$ and $e_2 > 0$). We also use equation (8) to compare the performance of the variable-length segment models to that of the single-segment model, which represents the entire fish body using one segment like a rigid plate. In swimming studies, rigid plates such as hydrofoils (Anderson *et al* 1998) are often used as a benchmark while evaluating the contribution of undulatory movements in propulsion.

2.6.5. Species comparison

We obtain a five-segment model to describe the swimming kinematics of every fish in the multi-species dataset. We study how segment lengths and motion parameters vary among the models. We hypothesize that the segment configuration of each species is related to its morphology. To begin to test this hypothesis, we check whether there is a correlation between head segment length (or the position of the most of anterior joint) and the maximum body width by fitting a linear regression using the least squares method. To evaluate whether there is a common propulsive strategy across fishes, we study a family of equations (e.g., linear regression, polynomials, power and exponential growth) to describe how pitch amplitude and phase varies across body segments (i.e., $\alpha_i, \varphi_i = f(r_i)$ where $i = 2, 3, 4, 5$). To minimize the risk of overfitting, we choose the simplest model with $R^2 > 0.9$. We check how much the head amplitude decreases while increasing segment length. To reconcile head and body kinematics, we also check whether there is a correlation between the head and the tail beat amplitudes.

2.6.6. Traditional kinematics analysis

During steady swimming, midline points oscillate from side to side at the tail beat frequency. For each species, we measure the peak-to-peak amplitude and timing (phase) of these oscillations to evaluate how midline points move with respect to each other. We estimate head and tail amplitudes from the first and last point along the midline, respectively. To calculate the body wavelength, we first estimate the body wave speed from the phase envelope (how phase values change along the body) and then divide the speed by the tail beat frequency. We also study body curvature (defined as the reciprocal of the radius of a circle) and how it changes along the midline. For each midline point, we calculate curvature by taking two adjacent points into account (one anterior and posterior). We average curvature values over time and report the maximum mean curvature and where it occurs along the body. We calculate the Spearman rank correlation to evaluate whether there is a statistical relationship between these kinematics variables and the segment lengths in five-segment multi-species models.

3. Results

There is a strong agreement between the models generated by the segment growing method and the

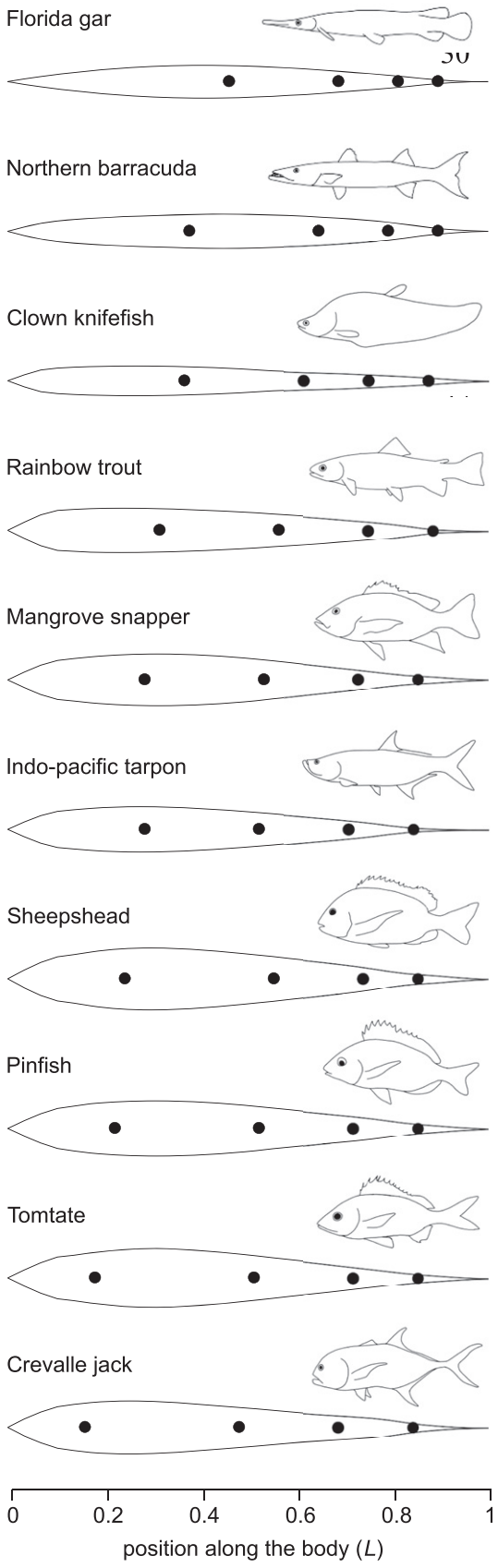

Figure 4. Optimal joint positions in five-segment models (multi-species dataset). Datasets are ordered according to the position of the most anterior joint (moving closer to the head from top to bottom). Fish silhouettes (both ventral and side views) are also shown.

genetic algorithm. For both datasets, the two algorithms converge on models with the same number of segments and joint positions (supplementary figure 4). Therefore, we only present results generated by the segment growing method to prevent repetition.

We find that those models with variable-length segments consistently perform better (i.e., producing a lower error) than the models with equal-length segments (figure 3(a)). While the error decreases with number of segments in a non-linear fashion (first rapidly and then slowly similar to an exponential decay), the decay rate is faster in the variable-length segment models ($b = -1.5 \pm 0.1$) than in the equal-length segment models ($b = -1.3 \pm 0.1$). This suggests that all else being equal, the variable-length approach produces more parsimonious models with fewer segments than the equal-length approach. For instance, a model with four variable-length segments is sufficient to mimic the actual fish midlines with less than $0.01L$ error (supplementary figure 5), whereas the equal-length approach requires at least two more segments (six segments in total) to achieve a similar result (supplementary figure 6). Otherwise, models with four equal-length segments fail to describe the movements of the posterior body adequately (in particular, towards the caudal fin see supplementary figure 7).

When using the same number of segments, the variable-length segment models outperform the equal-length segment models, for instance by 52% ($0.009 \pm 0.001\ L < 0.018 \pm 0.002\ L$, with the four-segment model), 59% ($0.006 \pm 0.001\ L < 0.015 \pm 0.002\ L$, with the five-segment model) and 55% ($0.004 \pm 0.001\ L > 0.010 \pm 0.002\ L$, with the six-segment model) (figure 3(b)). Compared to the single-segment model ($0.056 \pm 0.008\ L$, supplementary figure 8), four, five and six-segment models improve the performance by 85%, 90% and 92%, respectively (figure 3(c)).

We observe that, for the optimal performance, anterior segments should be longer than the posterior segments regardless of how many segments models may have (supplementary figure 9). Regarding models with up to five segments, the segments gradually become shorter as we move along the body, e.g., $0.39 \pm 0.05\ L\ (S_1) > 0.28 \pm 0.02\ L\ (S_2) > 0.18 \pm 0.01\ L\ (S_3) > 0.15 \pm 0.01\ L\ (S_4)$ in the four-segment model and $0.27 \pm 0.06\ L\ (S_1) > 0.26 \pm 0.03\ L\ (S_2) > 0.2 \pm 0.01\ L\ (S_3) > 0.14 \pm 0.01\ L\ (S_4) > 0.13 \pm 0.01\ L\ (S_5)$ in the five-segment model. In models with a bigger number of segments, we see the same trend apart from the first and the last segments, which are used to describe the head and caudal fin movements, respectively.

Our results from the multi-species dataset suggest that using five segments is more than sufficient to describe the kinematics of steady swimming (the average model error is $0.005 \pm 0.001\ L$). Similar to the trout dataset, we find that in all species the

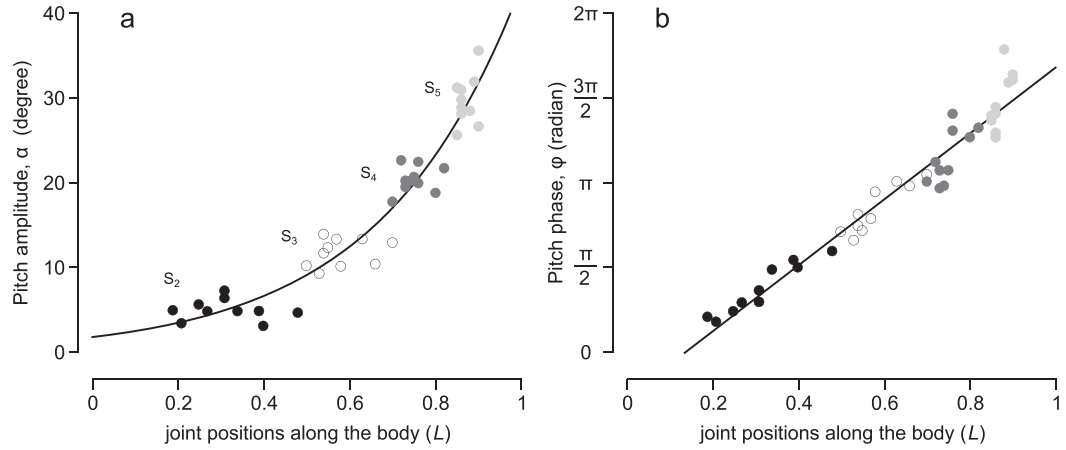

Figure 5. Control parameters for body segments S_2 (black circles), S_3 (white), S_4 (dark grey) and S_5 (light grey). Each data point corresponds to a measurement from different fish in the multi-species dataset. (a) Pitch amplitude ($y = 1.976e^{3.09x}$, $R^2 = 0.93$). (b) Pitch phase relative to the head segment ($y = 6.1x - 0.82$, $R^2 = 0.94$, $p < 0.01$).

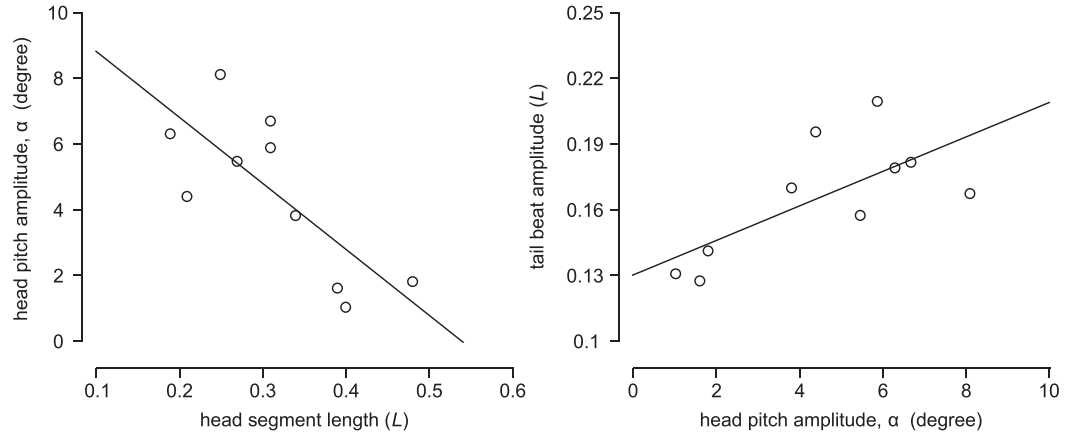

Figure 6. Analysis of head movements. (a) Pitch amplitude versus length ($y = -20.04x + 10.83$, $R^2 = 0.57$, $p < 0.05$). (b) Tail beat amplitude versus head pitch amplitude ($y = 0.01x + 0.13$, $R^2 = 0.49$, $p < 0.05$). Each data point (empty circles) corresponds to a measurement from different fish in the multi-species data set.

anterior segments are longer than the posterior segments (figure 4). However, there is a substantial variation among species in the way that the anterior body is partitioned. We find that wider fish have shorter head segments (supplementary figure 10). For instance, in the crevalle jack (maximum body width = 0.14 *L*) the head segment is short and ends at the base of the cranium (0.19 *L*), whereas in the Florida gar (maximum body width = 0.08 *L*) the head segment is much longer and spans half of the body (0.48 *L*). Moving along the body, we see less and less variation in the segment lengths. In particular, we note that the standard deviations from the mean length are 0.09 *L* (S_1), 0.06 *L* (S_2), 0.04 *L* (S_3) and 0.02 *L* (S_4).

Our kinematics analysis shows that the 10 (sub-) carangiform species studied here exhibit large variations in the kinematics parameters traditionally used to study steady swimming: speed (1 *L* s^{-1} – 3.1 *L* s^{-1}), body wavelength (0.7 *L* – 1.1 *L*), tail beat amplitude (0.12 *L*–0.21 *L*), head amplitude (0.01 *L* – 0.07 *L*), maximum curvature (3.3 *L* – 5.3 *L*) and maximum curvature point along the body (0.83 *L* – 0.9 *L*) (supplementary figure 11 and supplementary table 1). We see that these variations are reflected in the segment formation of our models (supplementary table 2); most notably, fish swimming with longer wavelength have longer segments in the posterior body.

We discover that as diverse as these fishes are one control strategy may unite them all. There exists a simple relationship between the location of a segment and how it moves, and this relationship does not change whether we study barracuda (elongated body), trout (fusiform body) or sheepshead (laterally compressed). For segments representing the fish body, pitch amplitude increases exponentially (figure 5(a)) and pitch phase increases linearly (figure 5(b)) in accordance with the joint position. For segments representing the head, pitch amplitude decreases with length: the longer the head, the smaller the pitch (figure 6(a)) and there is a coupling between head and body segments with a phase difference correlated with the position of the most anterior joint.

We also find a positive correlation between the head and tail beat amplitudes, where tail beat amplitude increases with head amplitude (figure 6(b)).

4. Discussions

We have described a novel approach which can automatically translate undulatory fish movements into empirical design guidelines for roboticists. In our approach, we first partition the fish body into a series of interconnected segments. We then study the relative movements of these segments with respect to each other. In this study, we have demonstrated the usefulness of this approach by analyzing the steady swimming kinematics of 10 (sub-)carangiform swimmers. We have presented the optimal segment formation and control parameters that allow accurate description of the kinematics of these fishes (table 2), and that can be used as a resource for future robotics work.

Below, we discuss our findings within the context of current fish robots described in the literature which vary in body lengths (from 17 to 66 cm), number of segments (from three to six), relative length of each segment (e.g., head segment length varies from 0.2 to 0.8 L), having rigid versus compliant segments and actuated versus passive joints (figure 7).

4.1. Accurate description of steady swimming kinematics with five segments

Our analysis suggests that five-segment models can approximate the undulatory movements of (sub-) carangiform swimmers during steady swimming with at least 99% accuracy (model error $<0.01L$). For optimal performance, the segments should become shorter moving towards the tail; this pattern is consistent for all species studied here. Although, there are not many fish robots designed this way, several studies have already showed that optimizing segment lengths (using real fish data) can improve the performance of freely swimming robots (Yu *et al* 2007).

How closely do robots need to mimic the midline kinematics of fishes? We have shown that the accuracy of multi-segment models increases with number of segments. However, we still do not know how segment number affects the actual performance of a robot, which is typically evaluated in terms of swimming speed and power efficiency. In other words, with all else being equal, can a five-segment robot swim faster than a four-segment robot without spending more energy? And if so by how much? Our modelling approach cannot directly address these questions as it does not consider internal and fluid forces while computing optimal segment formation. However, it offers reasonable starting points which may help exploring the design space more effectively. To systematically evaluate the swimming performance and hydrodynamic effects of different segment configurations, further experiments including physical robots (Yu *et al* 2007) and computational fluid dynamics simulations (Eloy 2013, Liu *et al* 2017) are required.

We recognize that it is not easy to manufacture robots with many small segments that are actuated independently. Perhaps it is not a coincidence that we see more robot designs which substitute posterior segments with a compliant body and a passive, flexible tail. In recent years, there is a growing amount of evidence suggesting that soft, underactuated fish robots can achieve better swimming performance than multi-segment rigid robots (Zhong *et al* 2018). However, to design and control these robots effectively, we need more comprehensive theoretical models which can link kinematics to interactions between motor commands, soft body properties and the fluid environment accurately (Zhong *et al* 2018, Epps *et al* 2009).

4.2. No proto-(sub-)carangiform swimmer

During steady swimming, fishes exhibit a wide range of undulatory kinematics that can be broadly classified into four swimming modes; anguilliform, sub-carangiform, carangiform and thunniform after (Breder 1926, Lindsey 1978). The majority of fish robots are designed after an abstract (sub-) carangiform swimmer with the following general design characteristics: the body has a fusiform shape, body amplitudes increase exponentially towards the tail, and the tail beat amplitude and body wavelength are assumed to be around 0.2 L and 1 L, respectively (Fiazza *et al* 2010). Here, we have shown that this simplified approach does not encapsulate the morphological and kinematics differences we observe in (sub-)carangiform swimmers. For instance, the body width, the tail beat amplitude and the body wavelength of the 10 species studied here vary greatly; their coefficient of variation (standard deviation divided by mean) are 0.24, 0.18 and 0.13, respectively. Similarly, the key locations where bending moments are applied (especially in the anterior part) are distinct for each species (the coefficient of variation is 0.28) and very likely stemming from differences in morphology. Our preliminary analysis between morphology and kinematics suggest that the maximum body width is a good predictor of the head segment length (wider fish have shorter head segments).

4.3. One body control strategy for all fishes

Our findings suggest that as diverse as (sub-) carangiform swimmers are, they may all use the same movement strategy to undulate. How much and when a segment moves is determined simply by its joint's location along the body and this relationship does not

Table 2. Optimal actuation points (where segments rotate around) and control parameters of five-segment models (multi-species dataset). Note that S_1 and S_2 have the same actuation points but face the opposite directions.

Species	S_1	S_2	S_3	S_4	S_5
Florida gar					
Actuation points (L)	0.48	0.48	0.7	0.82	0.9
Pitch amplitude (degree)	1.83	4.79	13.01	21.74	35.50
Pitch phase (radian)	0	1.88	3.30	4.15	5.13
Northern barracuda					
Actuation points (L)	0.4	0.4	0.66	0.80	0.90
Pitch amplitude (degree)	1.06	3.24	10.49	18.84	26.64
Pitch phase (radian)	0	1.58	3.08	3.98	5.04
Clown knifefish					
Actuation points (L)	0.39	0.39	0.63	0.76	0.88
Pitch amplitude (degree)	1.63	4.99	13.42	22.48	28.44
Pitch phase (radian)	0	1.72	3.16	4.41	5.6
Rainbow trout					
Actuation points (L)	0.34	0.34	0.58	0.76	0.89
Pitch amplitude (degree)	3.83	4.97	10.22	19.98	31.88
Pitch phase (radian)	0	1.54	2.97	4.09	4.99
Mangrove snapper					
Actuation points (L)	0.31	0.31	0.55	0.74	0.86
Pitch amplitude (degree)	6.69	6.50	12.41	20.22	28.82
Pitch phase (radian)	0	0.94	2.25	3.08	4.06
Indo-pacific tarpon					
Actuation points (L)	0.31	0.31	0.54	0.72	0.85
Pitch amplitude (degree)	5.88	7.36	13.99	22.65	31.17
Pitch phase (radian)	0	1.15	2.55	3.52	4.37
Sheepshead					
Actuation points (L)	0.27	0.27	0.57	0.75	0.86
Pitch amplitude (degree)	5.47	4.96	13.41	20.71	29.77
Pitch phase (radian)	0	0.93	2.48	3.37	4.53
Pinfish					
Actuation points (L)	0.25	0.25	0.54	0.73	0.86
Pitch amplitude (degree)	8.1	5.75	11.76	19.52	28.13
Pitch phase (radian)	0	0.77	2.35	3.37	4.42
Tomtate					
Actuation points (L)	0.21	0.21	0.53	0.73	0.86
Pitch amplitude (degree)	4.41	3.46	9.37	20.26	30.92
Pitch phase (radian)	0	0.58	2.08	3.04	3.98
Crevalle jack					
Actuation points (L)	0.19	0.19	0.5	0.7	0.85
Pitch amplitude (degree)	6.3	5.07	10.3	17.8	25.6
Pitch phase (radian)	0	0.67	2.24	3.16	4.29

change whether we study the movements of two different segments in the same fish or the same segments in two different fish. What separates fishes, however, are the joint locations where bending moments are applied. Once these locations are factored in, the kinematic diversity collapses into a single swimming pattern that is governed by a simple formula. What this means is that the same control algorithm can generate different swimming styles, simply by changing the segment formation. For instance, a robot can switch from swimming like a trout to swimming like a barracuda by lengthening the most anterior segment.

Fishes are tuned to swim with high swimming efficiency (Anderson *et al* 1998, Taylor *et al* 2003, Gazzola *et al* 2014, Nangia *et al* 2017). Our kinematics modelling is informative for roboticists as it provides clear guidelines on how to build a multi-segment robot and how body segments should move with respect to each other on the basis of biological evidence. However, it does not tell us how these movements can be realized in a real robot. We still do not know whether each segment should be actuated independently, or passive tail joints would suffice achieving fish-like bending kinematics. For instance, a recent study has shown that partitioning the tail with passive joints can reduce the cost of transport up to 50% in a tuna-inspired robot (White *et al* 2020). Similarly, in the case of hybrid robots with rigid body segments in the anterior body and compliant segments in the posterior body, our models are still informative while choosing the position of the anterior joints. In addition, once built, a robot will need a dynamic controller, which incorporates mechanical and hydrodynamic forces, to generate timely motor commands that can lead to the desired body movements. A number of control architectures featuring central pattern generators (Bal *et al* 2019), proportional-integral-derivative (Salumäe and Kruusmaa 2013) and fuzzy controllers (Liu and Hu 2006), and principles from Braitenberg vehicles (Salumäe *et al* 2012) have been successfully applied to drive fish robots.

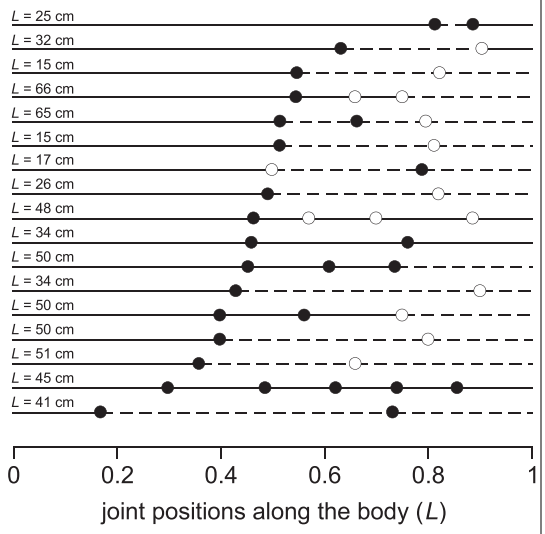

Figure 7. Current fish robot designs. Rigid (solid line) and compliant segments (dashed line). Actuated (filled circle) and passive joints (empty circle). Each joint controls the following segment on the right. The most anterior segment corresponds to the head segment. From top to bottom: (Zheng *et al* 2010, Long *et al* 2006, Wang *et al* 2008, Low and Chong 2010, Hirata 2000, Epps *et al* 2009, Gibouin *et al* 2018, Zhu *et al* 2019, Liu *et al* 2005, Hirata *et al* 2000, Liu and Hu 2006, Marchese *et al* 2014, Ay *et al* 2018, Kruusmaa *et al* 2014, Zhong *et al* 2017, Yu *et al* 2007, Rossi *et al* 2011). For each study, robot lengths are provided on the left. Note that this brief survey does not intend to summarize all fish robots discussed in the literature.

4.4. Active head control may improve swimming performance

We show here that longer fish rotate their head less (pitch amplitude decreases with increasing head length). In all fishes, head and body movements are coupled where body segments follow the lead of the head in a timely manner. These two relationships, in return, positively correlate with the variations we see in tail beat amplitude (e.g., fish with larger head oscillations have larger tail beat amplitudes).

We have recently observed a similar relationship in accelerating fishes (Akanyeti *et al* 2017). Our findings suggest the importance of head control in swimming, which is often overlooked when building fish robots. Until now, design efforts in robotics have mainly focussed on the control of the posterior body. In these robots, the head may constitute a large portion of the anterior body and it usually oscillates passively due to reaction forces and torques generated by the undulatory movements of the posterior body. In contrast, there is mounting evidence in the fish literature suggesting that timely head movements improve swimming performance, be it through reducing hydrodynamic drag (Lighthill 1969) or producing thrust (Gemmell *et al* 2016, Lucas *et al* 2020). Active head movements can also aid in directional control such as turning (Gray 1933), attacking prey (Nelson and Maciver 1999), feeding (Richard and Wainwright 1995), enhancing flow sensing (Akanyeti *et al* 2016).

4.5. Future work

We recognize that modelling fish movements in two-dimensions using a series of interlinked rigid body segments is rather simplistic. In reality, fish move in three-dimensions (e.g., cupping motion of the caudal fin) and modulate the stiffness of the body and fin rays in real-time to improve swimming efficiency (Long and Nipper 1996, Esposito *et al* 2012, Tytell *et al* 2010). It remains to be seen how optimal segment formation and control would change if the tail segment is allowed to be compliant, pitching and rotating at the same time.

Our comparative analysis on a multi-species dataset is limited to one individual swimming at one speed per species. Our ongoing work focuses on studying the effects of a fish's speed and size upon multiple individuals, and on characterizing the bending kinematics of anguilliform and thunniform swimmers. Our initial investigation from preliminary data suggests that our findings can be extended to describe the bending kinematics of thunniform swimmers accurately. In contrast, different segment formations (i.e., more equal-length segments) are needed to describe the kinematics of anguilliform swimmers; especially when they swim with shorter wavelengths (unpublished data).

We are also looking at how the bending kinematics of a fish change across behaviours (e.g., Kármán gaiting, accelerating forward to catch a prey, turning and escape responses). We predict that fast behaviours exhibiting large body amplitudes and curvatures (e.g., C-start) will require higher fidelity models with many segments than behaviours with subtle body movements (e.g., gliding). Similarly, the segment formation may vary dynamically during intermittent swimming such as burst and gliding where fish alternate periodically between forward linear acceleration and powerless gliding. Through these further studies, we can begin to build a comprehensive dictionary which translates the behaviour repertoire of fishes into pragmatic design solutions for roboticists.

Data

Fish midline data and our scripts are available on request. Table 1 presents the joint positions, pitch amplitude and pitch phase for each fish in the multi-species dataset (only for five-segment models). Supplementary table 1 presents the kinematics variables (including the body length and swimming speed) of each fish in the multi-species dataset.

Data availability statement

All data that support the findings of this study are included within the article (and any supplementary files).

Author contributions

SEAWF and OA conceived the research, develop the algorithms, analysed the data. OA wrote the first draft. SEAWF, QS and OA made the final edits.

Acknowledgments

This manuscript is dedicated to the memory of Mr. Martin Nelmes. We thank Dr. Alexandros Giagkos for useful discussions during the implementation of the genetic algorithm. We also thank Melissa O'Reilly and James Bradley Strong for commenting on the earlier version of the manuscript, and Allison Zwarycz for fish drawings in figure 4. This work is supported by Sefr Cymru Cofund II Research Fellowship Grant to OA and QS and by Knowledge Economy Skills Scholarship to OA and SEAWF. Both Grants were provided by European Social Funds through the Welsh Government.

ORCID iDs

Qiang Shen https://orcid.org/0000-0001-9333-4605
Otar Akanyeti https://orcid.org/0000-0003-3515-6833

References

Akanyeti O and Liao J C 2013 A kinematic model of Kármán gaiting in rainbow trout *J. Exp. Biol.* **216** 4666–77
Akanyeti O, Putney J, Yanagitsuru Y R, Lauder G V, Stewart W J and Liao J C 2017 Accelerating fishes increase propulsive efficiency by modulating vortex ring geometry *Proc. Natl Acad. Sci. USA* **114** 13828–33
Akanyeti O, Thornycroft P J, Lauder G V, Yanagitsuru Y R, Peterson A N and Liao J C 2016 Fish optimize sensing and respiration during undulatory swimming *Nat. Commun.* **7** 11044
Altringham J D and Ellerby D J 1999 Fish swimming: patterns in muscle function *J. Exp. Biol.* **202** 3397–403
Anderson J, Streitlien K, Barrett D and Triantafyllou M 1998 Oscillating foils of high propulsive efficiency *J. Fluid Mech.* **360** 41–72
Ay M, Korkmaz D, Ozmen Koca G, Bal C, Akpolat Z and Bingol M 2018 Mechatronic design and manufacturing of the intelligent robotic fish for bio-inspired swimming modes *Electronics* **7** 118
Bainbridge R 1963 Caudal fin and body movement in the propulsion of some fish *J. Exp. Biol.* **40** 23–56
Bal C, Korkmaz D, Koca G O, Ay M and Akpolat Z H 2016 Link length optimization of a biomimetic robotic fish based on big bang—big crunch algorithm *2016 21st Int. Conf. on Methods and Models in Automation and Robotics (MMAR)* (IEEE) pp 189–93
Bal C, Ozmen Koca G, Korkmaz D, Akpolat Z H and Ay M 2019 CPG-based autonomous swimming control for multi-tasks of a biomimetic robotic fish *Ocean Eng.* **189** 106334
Breder C Jr 1926 The locomotion of fishes *Zoologica* **4** 159–291
Eloy C 2013 On the best design for undulatory swimming *J. Fluid Mech.* **717** 48
Epps B P, Alvarado P V Y, Youcef-Toumi K and Techet A H 2009 Swimming performance of a biomimetic compliant fish-like robot *Exp. Fluids* **47** 927–39
Eriksen C C, Osse T J, Light R D, Wen T, Lehman T W, Sabin P L, Ballard J W and Chiodi A M 2001 Seaglider: a long-range autonomous underwater vehicle for oceanographic research *IEEE J. Ocean. Eng.* **26** 424–36
Esposito C J, Tangorra J L, Flammang B E and Lauder G V 2012 A robotic fish caudal fin: effects of stiffness and motor program on locomotor performance *J. Exp. Biol.* **215** 56–67
Fiazza C, Salumäe T, Listak M, Kulikovskis G, Templeton R, Akanyeti O, Megill W, Fiorini P and Kruusmaa M 2010 Biomimetic mechanical design for soft-bodied underwater vehicles *OCEANS'10 IEEE Sydney* (IEEE) pp 1–7
Gazzola M, Argentina M and Mahadevan L 2014 Scaling macroscopic aquatic locomotion *Nat. Phys.* **10** 758–61
Gemmell B J, Fogerson S M, Costello J H, Morgan J R, Dabiri J O and Colin S P 2016 How the bending kinematics of swimming lampreys build negative pressure fields for suction thrust *J. Exp. Biol.* **219** 3884–95
Gibouin F, Raufaste C, Bouret Y and Argentina M 2018 Study of the thrust–drag balance with a swimming robotic fish *Phys. Fluids* **30** 091901
Gray J 1933 Directional control of fish movement *Proc. R. Soc.* B **113** 115–25
Hirata K 2000 Development of experimental fish robot *Proc. of the 6th Int. Symp. Marine Engineering (ISME 2000)* pp 23–7
Hirata K, Takimoto T and Tamura K 2000 Study on turning performance of a fish robot *1st Int. Symp. on Aqua Bio-Mechanisms* 287–92
Jayne B C and Lauder G V 1995 Speed effects on midline kinematics during steady undulatory swimming of largemouth bass, micropterus salmoides *J. Exp. Biol.* **198** 585–602
Kruusmaa M *et al* 2014 FILOSE for svenning: a flow sensing bioinspired robot *IEEE Robot. Autom. Mag.* **21** 51–62
Lighthill M J 1969 Hydromechanics of aquatic animal propulsion *Annu. Rev. Fluid Mech.* **1** 413–46
Lindsey C 1979 Form, function and locomotory habits in fish *Locomotion* (New York: Academic)
Liu G, Ren Y, Dong H, Akanyeti O, Liao J C and Lauder G V 2017 Computational analysis of vortex dynamics and performance enhancement due to body–fin and fin–fin interactions in fish-like locomotion *J. Fluid Mech.* **829** 65–88
Liu J-D and Hu H 2006 Biologically inspired behaviour design for autonomous robotic fish *Int. J. Autom. Comput.* **3** 336–47
Liu J, Dukes I and Hu H 2005 Novel mechatronics design for a robotic fish *2005 IEEE/RSJ Int. Conf. on Intelligent Robots and Systems* (IEEE) pp 807–12
Liu J and Hu H 2010 Biological inspiration: from carangiform fish to multi-joint robotic fish *J. Bionic Eng.* **7** 35–48
Long J H Jr, Koob T J, Irving K, Combie K, Engel V, Livingston N, Lammert A and Schumacher J 2006 Biomimetic evolutionary analysis: testing the adaptive value of vertebrate tail stiffness in autonomous swimming robots *J. Exp. Biol.* **209** 4732–46
Long J H Jr and Nipper K S 1996 The importance of body stiffness in undulatory propulsion *Am. Zool.* **36** 678–94
Low K H and Chong C W 2010 Parametric study of the swimming performance of a fish robot propelled by a flexible caudal fin *Bioinsp. Biomim.* **5** 046002
Lucas K N, Lauder G V and Tytell E D 2020 Airfoil-like mechanics generate thrust on the anterior body of swimming fishes *Proc. Natl Acad. Sci. USA* **117** 10585–92
Marchese A D, Onal C D and Rus D 2014 Autonomous soft robotic fish capable of escape maneuvers using fluidic elastomer actuators *Soft Robot.* **1** 75–87
Nangia N, Bale R, Chen N, Hanna Y and Patankar N A 2017 Optimal specific wavelength for maximum thrust production in undulatory propulsion *PloS One* **12** e0179727
Nelson M E and Maciver M A 1999 Prey capture in the weakly electric fish apteronotus albifrons: sensory acquisition strategies and electrosensory consequences *J. Exp. Biol.* **202** 1195–203

Ozmen Koca G, Bal C, Korkmaz D, Bingol M, Ay M, Akpolat Z and Yetkin S 2018 Three-dimensional modeling of a robotic fish based on real carp locomotion *Appl. Sci.* **8** 180

Ribas D, Palomeras N, Ridao P, Carreras M and Mallios A 2011 Girona 500 AUV: from survey to intervention *IEEE/ASME Trans. Mechatronics* **17** 46–53

Richard B and Wainwright P 1995 Scaling the feeding mechanism of largemouth bass (micropterus salmoides): kinematics of prey capture *J. Exp. Biol.* **198** 419–33

Root R G, Courtland H-W, Shepherd W and Long J H Jr 2007 Flapping flexible fish *Exp. Fluids* **43** 779–97

Rossi C, Colorado J, Coral W and Barrientos A 2011 Bending continuous structures with SMAs: a novel robotic fish design *Bioinsp. Biomim.* **6** 045005

Salumäe T and Kruusmaa M 2013 Flow-relative control of an underwater robot *Proc. R. Soc.* A **469** 20120671

Salumäe T, Ranó I, Akanyeti O and Kruusmaa M 2012 Against the flow: a Braitenberg controller for a fish robot *2012 IEEE Int. Conf. on Robotics and Automation* (IEEE) pp 4210–5

Su Z, Yu J, Tan M and Zhang J 2014 Implementing flexible and fast turning maneuvers of a multijoint robotic fish *IEEE/ASME Trans. Mechatronics* **19** 329–38

Taylor G K, Nudds R L and Thomas A L R 2003 Flying and swimming animals cruise at a Strouhal number tuned for high power efficiency *Nature* **425** 707–11

Tytell E D, Hsu C-Y, Williams T L, Cohen A H and Fauci L J 2010 Interactions between internal forces, body stiffness, and fluid environment in a neuromechanical model of lamprey swimming *Proc. Natl Acad. Sci.* **107** 19832–7

Tytell E D and Lauder G V 2004 The hydrodynamics of eel swimming: I. Wake structure *J. Exp. Biol.* **207** 1825–41

Videler J and Hess F 1984 Fast continuous swimming of two pelagic predators, saithe (pollachius virens) and mackerel (scomber scombrus): a kinematic analysis *J. Exp. Biol.* **109** 209–28

Wang Z, Hang G, Li J, Wang Y and Xiao K 2008 A micro-robot fish with embedded SMA wire actuated flexible biomimetic fin *Sensors Actuators* A **144** 354–60

Wardle C, Videler J and Altringham J 1995 Tuning in to fish swimming waves: body form, swimming mode and muscle function *J. Exp. Biol.* **198** 1629–36

White C H, Lauder G V and Bart-Smith H 2020 Tunabot Flex: a tuna-inspired robot with body flexibility improves high-performance swimming *Bioinspiration Biomimetics* **16** 026019

Whitley D 1994 A genetic algorithm tutorial *Stat. Comput.* **4** 65–85

Yu J, Wang L and Tan M 2007 Geometric optimization of relative link lengths for biomimetic robotic fish *IEEE Trans. Robot.* **23** 382–6

Zheng C, Shatara S and Xiaobo T 2010 Modeling of biomimetic robotic fish propelled by an ionic polymer–metal composite caudal fin *IEEE/ASME Trans. Mechatronics* **15** 448–59

Zhong Y, Li Z and Du R 2017 A novel robot fish with wire-driven active body and compliant tail *IEEE/ASME Trans. Mechatronics* **22** 1633–43

Zhong Y, Song J, Yu H and Du R 2018 Toward a transform method from lighthill fish swimming model to biomimetic robot fish *IEEE Robot. Autom. Lett.* **3** 2632–9

Zhu J, White C, Wainwright D K, Di Santo V, Lauder G V and Bart-Smith H 2019 Tuna robotics: a high-frequency experimental platform exploring the performance space of swimming fishes *Sci. Robot.* **4** eaax4615